Lawrence Berkeley Laboratory
UNIVERSITY OF CALIFORNIA

Materials & Molecular Research Division

Submitted to Surface Science

A SURFACE CRYSTALLOGRAPHY STUDY BY DYNAMICAL LEED OF THE $(\sqrt{3}x\sqrt{3})R30^{\circ}$ CO STRUCTURE ON THE Rh(111) CRYSTAL SURFACE

R.J. Koestner, M.A. Van Hove, and G.A. Somorjai

September 1980

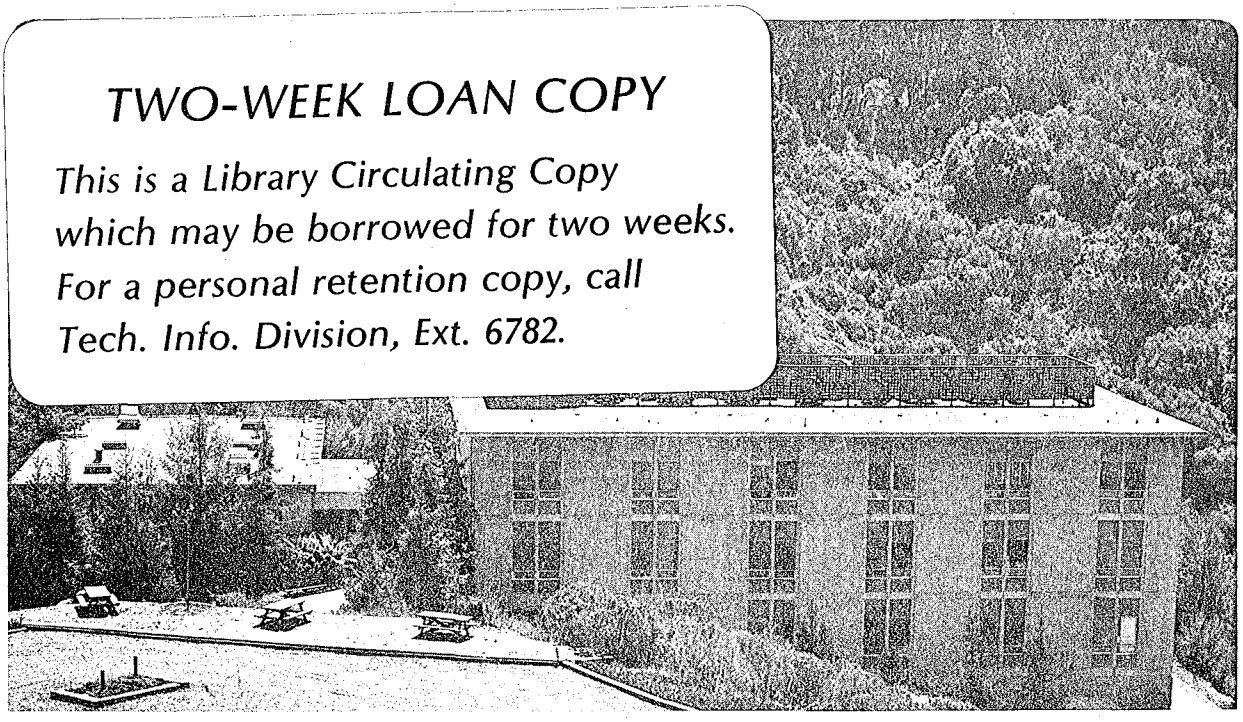

Prepared for the U.S. Department of Energy under Contract W-7405-ENG-48

A SURFACE CRYSTALLOGRAPHY STUDY BY DYNAMICAL LEED OF THE $(\sqrt{3}x\sqrt{3})R30°$ CO STRUCTURE ON THE Rh(111) CRYSTAL SURFACE

R.J. Koestner, M.A. Van Hove, and G.A. Somorjai

Materials and Molecular Research Division, Lawrence Berkeley Laboratory, and Department of Chemistry, University of California, Berkeley, CA 94720

Abstract

The atomic positions of the Rh(111)+$(\sqrt{3}x\sqrt{3})R30°$ CO and CO_2 surfaces are analyzed by dynamical LEED. The Rh(111)+$(\sqrt{3}x\sqrt{3})R30°$ CO and CO_2 systems produce identical I-V curves, confirming the dissociation of CO_2 to CO on this surface. The adsorbed CO is found to stand perpendicular to the surface with the carbon end down at an atop site (that is, terminally bonded). The CO overlayer spacings are d_{RhC}= 1.95$\pm$ 0.1 Å and d_{CO}=1.07$\pm$0.1Å. This geometry yields a Zanazzi-Jona R-factor of 0.40 and a Pendry R-factor of 0.50.

Introduction

There have been only a few low energy electron diffraction (LEED) intensity analyses carried out to determine the structure of molecules adsorbed on metal surfaces; most surface crystallography studies concentrated on the structure of adsorbed atoms on low Miller index, transition metal faces. The few molecular adsorption systems already investigated by dynamical LEED are CO on Ni(100)[1], Cu(100)[1c,1d] and Pd(100)[2] as well as C_2H_2 and C_2H_4 on Pt(111).[3] We report a similar study on the Rh(111)-$(\sqrt{3}x\sqrt{3})R30°$ CO and CO_2 systems.

CO adsorption on Rh(111) has already been studied by a variety of complementary techniques. Grant and Haas,[4] using LEED and Auger electron spectroscopy (AES), were the first to investigate CO and CO_2 adsorbed on Rh(111); they saw a (2x2) LEED pattern for CO and a 'split' (2x2) for CO_2. Castner et al.[5] observed a series of LEED patterns to appear with increasing CO coverage. The progression is a $(\sqrt{3}x\sqrt{3})R30°$ at $\theta=1/3$, a split (2x2) at $1/3 \leq \theta \leq 3/4$, and a (2x2) pattern at $\theta=3/4$. The patterns were interpreted as a continuous compression of a hexagonal overlayer of CO molecules in the coverage range $1/3<\theta<3/4$. The order-order transition from the split (2x2) structure was noted to be reversible with coverage and temperature, and thermal desorption spectra (TDS) showed first-order desorption kinetics with only one CO peak detectable. CO_2, although requiring a 5-10-fold higher gas exposure, has an identical progression of LEED patterns and identical thermal desorption spectra as CO, suggesting dissociative chemisorption into an oxygen atom and a CO molecule. The fate of this oxygen atom was not further investigated.

Strong evidence that the oxygen atom, derived from dissociated CO_2, dissolves into the rhodium lattice was found by Thiel et al.[6] At least 40% of the saturation coverage of O_2 on Rh(111) must be present before any O_2 desorption with increasing temperature can be measured; the large fraction of adsorbed oxygen that does not desorb dissolves into the crystal. They also saw a residual oxygen peak in the Auger electron spectrum after a high temperature crystal heating of the Rh(111)$\pm$(2x2) O structure, indicating roughly a 1 atom% concentration near the surface; this residual oxygen peak had a very different line shape from chemisorbed oxygen, and the peak could not be reduced by extended heat treatments or H_2/CO adsorptions. More recently, Thiel and coworkers[7] detected a low coverage (θ=1/4) (2x2) LEED pattern for CO adsorbed on Rh(111).

Dubois and Somorjai,[8] using high resolution electron energy loss spectroscopy (HREELS) in combination with LEED conclude that CO and CO_2 adsorb only at top sites ("terminal bonding") with the carbon end down at θ=1/3, begin populating the bridge-bonded positions in the $1/3<\theta<3/4$ coverage range, and finally occupy about twice as many top as bridge sites at the saturation coverage of θ=3/4. The order-order transition of the $(\sqrt{3}x\sqrt{3})R30°$ to the split (2x2) pattern was shown also to be reversible. In addition, they studied CO chemisorption on pretreated Rh(111). H_2 pre- or post-adsorption at room temperature had no noticeable effect on the vibrational or thermal desorption spectra; while O_2 and carbon pre-adsorption blocked possible CO adsorption sites as well as weakening the metal-CO bond and strengthening the CO bond. Interestingly, the O_2 pre-treated surface inhibited the bridge-bonded species from appearing while the carbon pretreated surface inhibited the atop species. Further evidence

for the dissociation of chemisorbed CO_2 on Rh(111) came from the observation that the adsorbed CO and CO_2 vibrational loss spectra were identical.

We report here a full dynamical LEED analysis with reliability factors for the Rh(111)+($\sqrt{3}$x$\sqrt{3}$)R30° CO and CO_2 surfaces. The I-V curves for CO and CO_2 adsorption are found to be identical, giving further evidence that CO_2 dissociates into CO on the Rh(111) surface. Our determination of the ($\sqrt{3}$x$\sqrt{3}$) R30° CO structure provides a necessary check on the proposed correlation between adsorbed CO vibrational frequencies and its adsorption sites on fcc(111) metals; it also yields a calibration of the vibrational loss spectroscopies, which makes their predictions at different coverages, in different ordering states, and on different substrate faces more reliable.

Experimental

The rhodium crystal of >99.9% purity was cut to within 1/2° of the (111) plane and mechanically polished to a ∿1μm diamond paste. The crystal was mounted on rhodium foil that in turn was attached to a Varian manipulator; the "flip" mechanism available was modified to allow an azimuthal rotation of about 90°. Before the manipulator was inserted into the UHV chamber, the crystal surface normal and the azimuthal rotation axis were made parallel to within 1/2° by laser reflection. The vacuum system is equipped with four-grid LEED/Auger optics, glancing incidence Auger electron gun, and a mass spectrometer head; the base pressure remained at ∿1x10^{-9} Torr during the experiments with the major background gases being H_2 and CO.

The crystal orientation (θ=0° and $\theta\neq$0°, ϕ=0°) was determined by

checking for the degeneracy of beam I-V profiles; an engraved scale on the manipulator head would allow an accurate (within 0.1°) displacement of the polar angle (θ) from normal incidence (θ=0°). With the LEED beam at normal incidence, a 6-fold degeneracy should exist for the (1/3,1/3) beams because of the mirror-plane and rotational symmetry of the $(\sqrt{3}x\sqrt{3})$R30° CO, CO_2 unit cell on the Rh(111) surface. (Even if the basis of the $(\sqrt{3}x\sqrt{3})$R30° unit cell had a lower symmetry, equivalent domains would regenerate the full symmetry in the diffraction pattern.) The (2/3, -1/3), (-1/3, -1/3), and (1/3,-2/3) beam profiles are indeed nearly degenerate at the assigned θ=0° orientation (Figure 1). Similarly at $\theta \neq 0°$, ϕ=0° (that is, when the projection of the incident LEED beam on the crystal face is parallel to the $[11\bar{2}]$ direction), there should be a mirror symmetry about the plane containing the surface normal and this $[11\bar{2}]$ direction. Figure 2 shows that this symmetry is nearly realized in the experiment.

The I-V curves were collected using the photographic method previously described.[9] The Nikon F camera was adjusted to an aperture of f1.8 and a shutter time of 1/2 sec; a high speed Kodak film (pan film 2484) was used. Four independent beam profiles, ranging from 44-224 eV were obtained for the clean Rh(111) surface at θ=0°; these curves are identical to those published previously by others.[10] The analysis of these experimental clean Rh(111) I-V curves will be published elsewhere.[11] A total of 27 independent profiles, ranging from 24-144 eV, were obtained for the Rh(111)+$(\sqrt{3}x\sqrt{3})$R30° CO, CO_2 system at three different incidence angles (θ=0°; θ=10°, ϕ=0°; and θ=20°, ϕ=0°); most of these CO I-V curves are plotted in the Appendix. The I-V profiles for the CO overlayer were reproduced in a second independent experiment. These curves were also reproduced by the Rh(111)+$(\sqrt{3}x\sqrt{3})$R30° CO_2

system (Figure 3). This not only supports the expectation that CO_2 dissociates into CO on this surface, as discussed in the Introduction, but provides an independent check on the I-V curves for adsorbed CO.

The experience gained in the analysis of Ni(100)+c(2x2)CO by Andersson and Pendry[1a] and by other authors[1b-f] led us to take special precautions in this work. Three difficulties were encountered in the CO/Ni analysis. First, the ordering of CO on Ni(100) is very sensitive to surface perfection and cleanliness. Second, there was a considerable decrease of intensity ($\sim$30% for the (1/2,1/2) beam) in the extra diffraction spots during the time needed to collect the I-V curves with a telephotometer. Third, the c(2x2) pattern nucleates (island formation) quickly. The extra diffraction spots would reach near maximum intensity far before the optimal coverage of θ=1/2. In light of this Ni(100)+c(2x2) CO work, we paid particular attention to the surface cleanliness of the Rh(111) crystal, the LEED beam induced damage of the CO overlayer, and the optimal exposure values for the ($\sqrt{3}$x$\sqrt{3}$)R30° structure.

An Auger electron spectrum of the crystal after only a few cleaning cycles showed substantial sulfur and boron as well as smaller chlorine and carbon peaks (Figure 4a). Boron (a 17 ppm bulk impurity) proved most troublesome to remove; only after weeks of continuous Ar^+ bombardments (1-3 amps, 1.2 kV) with five minute annealing at 800°C and O_2 treatments (flowing 5×10^{-7} Torr O_2, 700°C) was it largely depleted from the near surface region. Auger electron spectra taken during the CO and CO_2 adsorptions still revealed small contaminant peaks (S, B, C, Cl (See Fig.4b)); even months after this study was completed, with many additional cleaning cycles done, the amount of surface impurities had not been further reduced.

It should be noted that the residual probably subsurface oxygen seen by Thiel et al.[6] after O_2 treatments, is just below the detectability limit of our retarded-field Auger electron spectra; the expected residual oxygen peak ($O_{515}/Rh_{256} \sim 1.5\%$) is comparable with the noise level near 515 eV in our spectra (see Fig.4b,4c). It should be noted that although a substantial carbon peak is measured no oxygen peak is detected in the Auger electron spectra of the Rh(111)+$(\sqrt{3}x\sqrt{3})$R30° CO surface (Fig.4c); the expected O_{515}/Rh_{256} ratio is roughly 10%--a value significantly above the observed noise level of about 2-3%. This ratio is estimated from the Rh and oxygen peak height ratio measured for the Rh(111)+(2x1)-O structure with coverage θ=1/2.[12] We believe that this discrepancy is due to the incident Auger electron beam (2.2KeV, ~20μamps) induced fragmentation of the adsorbed CO and subsequent dissolution of the atomic oxygen. In fact, the higher coverage Rh(111)+(2x2) CO (θ=3/4) presently under study shows the same effect even more dramatically.

The LEED beam would first slightly improve the ordering of the overlayer structure; then an exponential decay with electron exposure would start in the extra diffraction spots. Figure 5 shows this decay for the (1/3,1/3) beam intensity. There seems to be two distinct decay rates at different electron exposures, although this was not further investigated. In light of this, the electron beam damage was minimized by moving the electron beam across the crystal during photography[1b,1c] thus limiting the electron exposure of any given region of the surface to about 40 μamp-secs As a result, the LEED spots would actually increase somewhat in intensity ($\lesssim$5-10%), thus indicating that with this exposure the exponential decay was not sufficient to offset the initial improvement in the ordering.

A further check on our data is provided by the absence of detectable discontinuities in the I-V profiles at the energies where the electron beam was moved to a different region of the surface. In addition, the independent experiments to check for reproducibility had staggered energy intervals to insure that no false peaks would arise at the joining energies.

The gas exposure could not be accurately measured with the needle doser used, but a constant CO pressure burst would repeatedly produce a sharp, intense LEED pattern with low background. Thiel et al.[7] found that the (1/3,1/3) beam intensity falls to half-maximum with a 15-20% over- or underexposure of CO, showing that the coverage can be fairly accurately determined by just checking the quality of the resulting LEED pattern. In addition, the CO_2 gas exposure was about 10-fold larger than the CO, but still produced identical I-V curves. If our overlayer coverage had been poorly controlled and if the I-V profiles were sensitive to CO coverage, we would not expect the CO and CO_2 beam profiles obtained in different gas exposure regimes to be identical. It should be mentioned that small amounts of H_2 and ambient CO were adsorbed on the crystal during liquid nitrogen cooling to -30°C (∿10 minutes) prior to CO or CO_2 exposure. Then, after adsorption of CO or CO_2, a crystal heating to 10-25°C would desorb H_2 and considerably sharpen the LEED spots.

3. LEED Theory

We apply established dynamical LEED formalism in our theoretical analysis of the I-V curves.[13] In particular, renormalized forward scattering is used between individual atomic layers, which include separate carbon and oxygen layers. The rhodium atoms are represented by a band structure muffin-tin potential,[14] which has been used successfully in other work on Rh(111).[10a,b]

For the C and O atoms X_α muffin-tin potentials calculated for a NiCO cluster have been chosen as these produced good LEED results on a nickel substrate.[1e] We also tried the C and O atomic potentials used in other CO/Ni work with LEED[1b] but found no material improvement in our results. The muffin-tin zero was initially set at -10 eV with respect to the vacuum level and then adjusted to -8 eV to best fit the clean Rh(111) I-V curves as described elsewhere.[11] This value is not further changed in the presence of the CO layer, since the work function change is negligible. Furthermore, /the CO layer is given the same muffin-tin zero as the substrate, since a change was tested for CO on Ni(100)[15] and on Pd(100)[2] but proved to have little effect at the energies under consideration. An imaginary part of the potential proportional to $E^{1/3}$ was chosen by observation of the peak widths in the experimental I-V curves. Rhodium thermal vibration amplitudes were increased by a factor of 1.4 relative to the bulk value for Rh, while the adatoms were given double the bulk rhodium vibration amplitudes. Variation of these amplitudes had a negligible effect on the structural determination.

Theory and experiment are compared through a set of R-factors and their average. These are[11]

ROS = fraction of energy range with slopes of opposite signs in the experimental and theoretical I-V curves; (1)

$$R1 = 0.75 \int |I_e - cI_t| dE / \int |I_e| dE; \quad (2)$$

$$R2 = 0.5 \int (I_e - cI_t)^2 dE / \int I_e^2 dE; \quad (3)$$

$$RRZJ = 0.5 \int \{|I_e'' - cI_t''|\ |I_e' - cI_t'| / (|I_e'| + \max|I_e'|)\} dE / (0.027 \int |I_e| dE); \quad (4)$$

$$RPE = 0.5 \int (Y_e - Y_t)^2 / \int (Y_e^2 + Y_t^2), \quad Y(E) = L/(1 + V_{0i}^2 L^2), L = I'/I \quad (5)$$

(5)

Here $c=\int|I_e|dE/\int|I_t|dE$; the apostrophe designates differentiation with respect to the energy. RRZJ is the reduced Zanazzi-Jona R-factor,[16] while RPE is Pendry's R-factor,[17] both renormalized with a factor 0.5 to match the scale of the other R-factors.

While the final R-factor value for a given surface structure is obtained by averaging over all available beams with weights proportional to each beam's energy range, we also exploit in the structural search the differences between R-factors for different beams. This is because different beams should simultaneously show minima when the correct surface structure is used, while with incorrect geometries it would be improbable to obtain this coincidence of minima. The justification for this is described in Ref.11. In short, in the kinematic limit each beam is sensitive to the projection of the atomic positions onto the direction of the particular momentum transfer vector corresponding to that beam. Therefore, it would be unlikely, even after multiple scattering is allowed for, that a particular incorrect surface geometry could have correct projections onto every available momentum transfer direction and produce R-factor minima in each beam.

Finally, the experimental curves were smoothed twice with a single three point smoothing formula. Both theory and experiment were also multiplied by an exponential function to give the high energy intensities weights equal to the low energy intensities and thus compensate for the intensity reduction due to thermal vibrations and the scattering amplitudes.

4. Results and Discussion

The clean Rh(111) surface was confirmed to have the ideal bulk structure, as described elsewhere,[11] with a Zanazzi-Jona R-factor value

(2xRRZJ) of 0.14 and a Pendry R-factor value (2xRPE) of 0.20. For the Rh(111)+ ($\sqrt{3}$x$\sqrt{3}$)R30° CO structural determination, four adsorption sites were analyzed which may be labelled aaABC...(top site), bbABC...(hcp hollow site), ccABC... (fcc hollow site), and ddABC...(bridge site). The CO molecule was kept perpendicular to the surface. The hollow sites were easily ruled out by comparison of normal incidence I-V curves. Beam dependent R-factors for the top and bridge sites are plotted in Fig.6 in the case of the θ=10° incidence direction. Variations in both the Rh-C and the C-O distances are included. It is easy to spot in Fig.6 that coincidence of beam R-factor minima does not occur for any reasonable geometry of the bridge site; whereas coincidence is easily recognized for the top site with interlayer spacings of $d_{RhC} \simeq 1.9$ Å and $d_{CO} \simeq 1.1$ Å. This geometry is illustrated in Fig.7.

More precise values for the interlayer spacings can be obtained as described in Ref.18. Consider the two-dimensional space of the variables d_{RhC} and d_{CO}. For each d_{RhC} the value of d_{CO} giving the smallest average R-factor is plotted; thereby a line of minima is produced. Similarly, for each d_{CO} the value of d_{RhC} giving the smallest average R-factor is plotted, producing a second line of minima. These two lines interesect in the desired overall minimum. If the average R-factor near this minimum is taken to have a quadratic dependence on d_{RhC} and d_{CO}, the two lines in question are straight and a graphical determination of the position of the minimum is straightforward, while points on the straight lines are easily determined by parabolic interpolations. In this fashion, the θ=0° data produce a minimum average R-factor (using ROS, R1, R2, RRZJ, and RPE) near (d_{RhC}, d_{CO})=(2.01, 1.02) Å, while the θ=10° and θ=20° data produce minima at (1.945, 1.075) Å and (1.945, 1.085) Å, respectively. Averaging with weights proportional to the amount of

data at each angle of incidence produces values of d_{RhC}=1.95± 0.1 Å, and d_{CO}=1.07±0.1 Å, where the conventional uncertainty of LEED analyses is quoted. We visually interpolate the average R-factor values at the minimum to 0.25 at θ=0°, 0.20 at θ=10°, and 0.26 at θ=20°, averaging out at about 0.23. The corresponding Zanazzi-Jona R-factor is about 0.40 for this structure; the Pendry R-factor is about 0.50 which is to be compared with about 0.50 and 0.40 for CO on Ni and Cu(100).[1d] Representative I-V curves are shown in Fig.8.

It is interesting that the best Zanazzi-Jona R-factor for the bridge site is only slightly larger than that for the top site (about 0.42 to 0.40); whereas the other R-factors clearly favor the top site (on the average by about 0.30 to 0.23). Thus a conventional analysis using just the Zanazzi-Jona R-factor would not be considered decisive. This is a strong argument in favor of (1) using more than one R-factor, and (2) using the coincidence of beam R-factor minima for distinguishing between two local minima in the average R-factor.

An additional structural feature that was tested is the topmost Rh-Rh interlayer spacing, which was found to be indistinguishable from the clean surface case, i.e. essentially bulk-like.

We observe in the R-factor dependence on d_{RhC} and d_{CO} a feature already noted by Andersson and Pendry[1d] for CO on Ni(100); an R-factor contour plot around the minimum can have an elongated elliptical shape with a major-to-minor axis ratio of up to ∿4:1. This elongation implies an uncertainty in the carbon position, but not in the oxygen postion, as can also be seen by the constancy of the optimum Rh-O distances found at our three incidence directions (3.03, 3.02, and 3.03 Å at θ=0, 10, and 20°

respectively), while the C position varies by 0.07 Å. The idea of shadowing of the C atoms by the overlying O atoms put forward by Andersson and Pendry may be correct; however, our data sample shows more momentum transfer space farther away from the surface normal than theirs and should, therefore, be less susceptible to such shadowing.

The uncertainty in the carbon position may explain the slight discrepancy between our result (d_{RhC}=1.95 Å, and d_{CO}=1.07 Å) and known Rh-C and C-O bond lengths in rhodium carbonyls, which range from 1.82 to 1.91 Å, and from 1.09 to 1.17 Å, respectively, according to a tabulation for terminal bonding in 10 different such carbonyl cluster.[19] In those clusters the Rh-O distance ranges from 2.96 to 3.04 Å. Thus our determination puts the C atom somewhat far from the metal, but not the O atom.

The slightly too small C-O interlayer distance may also be explained[1a] as due to the molecular axis bending away from the surface normal. However, it is difficult to understand an overestimated Rh-C distance with an argument of this kind.

The discrepancy in the case of CO on Rh(111) might also be ascribed to beam damage, as it was for the first CO/Ni(100) analysis. There a rather smaller CO interlayer spacing of 0.95 Å was obtained. However, we have taken special precautions in this respect, as described in Section 2. In addition, the CO/Pd(100) system suffered at least as much beam damage as the present one (as witnessed by clearly observable discontinuities between segments of I-V curves measured at different spots on the Pd sample), but produced very reasonable bond lengths, in particular 1.15 Å for the C-O distance. Furthermore, that study did not use beams emerging at large polar angles. Thus it is not at all clear where the uncertainty in our carbon

position comes from and whether it can be correlated with beam damage or with a lack of large polar-angle data.

Clearly the level of agreement that we obtain between theory and experiment is not of the best quality, but according to the Pendry R-factor it is essentially the same as Andersson and Pendry ultimately reached with CO on Ni(100). Probably improvements in either theory or experiment for CO on Rh(100) would reduce the uncertainty in the carbon position. However, our various tests do not indicate where an improvement is required.

Our result of top site adsorption for Rh(111)+($\sqrt{3}$x$\sqrt{3}$)R30°CO serves as a confirmation of the postulated correspondence in vibrational loss work between adsorption site and frequency range for CO adsorbed on different metal surfaces. Our result extends this confirmation to other than the fcc(100) substrate face, for which it was established with CO on Ni, Cu, and Pd(100). A summary of these results is shown in Table I. It is seen that the CO stretching frequency in the Rh(111)+($\sqrt{3}$x$\sqrt{3}$)R30° structure is closer to the frequency range associated with a bridge-gonded CO molecule than that for CO on Ni or Cu(100). Such confirmations provide an important calibration of the vibrational loss techniques in the sense that the knowledge of the CO adsorption site of one coverage or on one crystal face can be used to determine, without the help of further LEED intensity analyses, the adsorption site (but not necessarily the bond lengths and angles) at other coverages or in disordered states or on other substrate faces.

The identity, within experimental error, of the I-V curves measured for CO and CO_2 adsorption on Rh(111) provides a strong confirmation of the belief derived from TDS and HREELS work that CO_2 decomposes to CO and O, the CO taking the same structure as that described above for gaseous CO adsorption. The fate of the oxygen may be speculated upon in the light of the

similarity in I-V curves. One has to account for 1/3 of a monolayer of oxygen. It is hard to imagine this oxygen settling in the immediate subsurface region of the rhodium without affecting the I-V curves at least through a slight change in average Rh-Rh interlayer spacings, which we have tested. If the oxygen were interstitially located between the CO molecules on top of the substrate, the restricted available space would produce at least some degree of ordering of the oxygen atoms in a $(\sqrt{3}x\sqrt{3})R30°$ pattern and would thereby presumably affect the measured I-V curves. However, we found that the Rh(111)+$(\sqrt{3}x\sqrt{3})R30°$ CO and CO_2 surfaces produce identical I-V profiles. Since neither TDS nor HREELS ever detects this oxygen, it seems likely that it diffuses deep into the substrate.

Conclusion

For the Rh(111)+$(\sqrt{3}x\sqrt{3})R30°$ CO system, CO was found to be terminally bonded perpendicular to the surface. The best fit interlayer spacings for the CO overlayer are d_{RhC}=1.95 $\pm$ 0.1 Å and d_{CO}=1.07$\pm$0.1 Å. The corresponding R-factors of this geometry are 0.40 for the Zanazzi-Jona factor (2xRRZJ) and 0.50 for the Pendry factor (2xRPE); these values are comparable with the Pendry R-factors 0.50 and 0.40 obtained for CO on Ni and Cu(100),[1d] respectively.

The CO- and CO_2- derived I-V curves are identical; this gives further evidence that the adsorbed CO_2 dissociates into a CO molecule and an oxygen atom. There is no identifiable trace of this oxygen in the I-V curves, supporting the claim that this oxygen dissolves into the substrate.

The Zanazzi-Jona R-factor did not adequately distinguish between the top (0.40) and the bridge (0.42) site adsorption models. However, the

other R-factors clearly favor the top site (on the average by about 0.30 to 0.23), and the coincidence of the individual beam R-factor minima with only the top site geometry also provided a clear discrimination among the structural models tested.

The R-factor contours around the minimum in the d_{RhC}-d_{CO} plane imply a larger uncertainty in the Rh-C spacing than for the Rh-O spacing. To further support this observation, the Rh-O distance obtained agrees well with organometallic cluster compound values and is well reproduced in the different polar-angle data, while the Rh-C distance appears slightly too large when compared to the organometallic compounds and is not as well reproduced in the different polar-angle data.

Our result of the top site adsorption for Rh(111)-($\sqrt{3}$x $\sqrt{3}$)R30° CO extends the postulated correlation in vibrational loss spectroscopies between the adsorption site and the adsorbed CO vibration frequency range to fcc(111) metal surfaces.

Acknowledgement

This work was supported by the Division of Materials Science, Office of Basic Energy Sciences, U. S. Department of Energy under Contract W-7405-ENG-48.

References

1a. S. Andersson and J.B. Pendry, Surface Sci. 71 (1978) 75.

1b M. Passler, A. Ignatiev, F. Jona, D.W. Jepsen, and P.M. Marcus, Phys. Rev. Lett. 43 (1979) 360.

1c. S. Andersson and J.B. Pendry, Phys. Rev. Lett. 43 (1979) 363.

1d. S. Andersson and J.P. Pendry, J. Phys. C (in press).

1e. S.Y. Tong, A. Maldonado, C.H. Li, and M.A. Van Hove, Surface Sci. 94 (1980) 73.

1f. K. Muller, E. Lang, P. Heilmann, and K. Heinz, to be published.

2. R.J. Behm, K. Christmann, G. Ertl, M.A. Van Hove, P.A. Thiel, and W.H. Weinberg, Surface Sci. 88 (1979) L59.

3a. (for the metastable species) L.L. Kesmodel, R.C. Baetzold, and G. A. Somorjai, Surface Sci. 66 (1977) 299.

3b (for the stable spe .es) L.L. Kesmodel, L.H. Dubois, and G.A. Somorjai, J. Chem. Phys. 70 (1979) 2180.

4. J.T. Grant and T.W. Haas, Surface Sci. 21 (1970) 76.

5. D.G. Castner, B.A. Sexton, and G.A. Somorjai, Surface Sci. 71 (1978) 519.

6. P.A. Thiel, J.T. Yates, Jr., and W.H. Weinberg, Surface Sci. 82 (1979) 22.

7. P.A. thiel, E.D. Williams, J.T. Yates Jr., and W.H. Weinberg, Surface Sci. 84 (1979) 59.

8. L.H. Dubois and G.A. Somorjai, Surface Sci. 91 (1980) 514.

9a. P.C. Stair, T.J.Kaminsika, L.L. Kesmodel, and G.A. Somorjai, Phys. Rev. B11 (1975) 623.

9b. M.A. Van Hove, R.J. Koestner, P.C. Stair, J.P. Biberian, L.L. Kesmodel, I. Bartos, and G.A. Somorjai, Surface Sci., to be published.

References (continued)

10a. D.C. Frost, K.A.R. Mitchell, F.R. Shepherd, and P.R. Watson, Proc. 7th IVC and 3rd ICSS, Vienna, 2725 (1977).

10b. K.A.R. Mitchell, F.R. Shepherd, P.R. Watson, D.C. Frost, Surface Sci. 64 (1977) 737.

10c. C. Chan, P.A. Thiel, J.T. Yates Jr., and W.H. Weinberg, Surface Sci. 76 (1978) 296.

11. M.A. Van Hove and R.J. Koestner, Proc. Conf. on Determination of Surface Structure by LEED, Plenum Press (New York) 1981.

12. D.G. Castner and G.A. Somorjai, Surface Sci.

13. M.A. Van Hove and S.Y. Tong, Surface Crystallography by LEED, Springer-Verlag, Heidelberg, 1979.

14. V.L. Moruzzi, A.R. Williams, and J.F. Janak, Calculated Electronic Properties of Metals, Pergamon (New York) 1978.

15. M.A. Van Hove, unpublished.

16. E. Zanazzi and F. Jona, Surface Sci. 62 (1977) 61.

17. J.B. Pendry, J. Phys. C13 (1980) 937.

18. D.L. Adams, H.B. Nielsen, and M.A. Van Hove, Phys. Rev. B 20 (1979) 4789.

19. P. Chini, V. Longoni, and V.G. Albano, Adv. Organomet. Chem. 14 (1976) 285.

20. See, N. Sheppard and T.T. Nguyen, in Advances in Infrared and Raman Spectroscopy, Vol. 5 (R.J.H. Clark and R.E. Hester, eds.) Heyden and Son, London, 1978, 67.

21. S. Andersson, Solid State Commun. 27 (1977) 75.

22. C. Andersson, in Proc. 2nd European Conf. Surface Sci., Cambridge, 1977.

Figure Captions

1. Nearly degenerate beams at assigned $\theta=0°$ orientation. (Minor discrepancies pointed out by arrow head.)
2. Nearly degenerate beams at assigned $\phi=0°$ orientation.
3. Identity of CO and CO_2 derived I-V curves.
4. Auger electron spectra.
5. (1/3,1/3) Beam intensity decay with electron exposure.
6. Plot of individual beam R-factor minima with respect to d_{RhC} and d_{CO}.
7. Structure of Rh(100)+($\sqrt{3}$x$\sqrt{3}$)R30° CO.
8. Comparison between experimental (dark) and theoretical (light) I-V curves for (a) $\theta=0°$, (b) $\theta=10°$, $\phi=0°$, and (c) $\theta=20°$, $\phi=0°$.

Appendix

Rh(100)+(v3xv3)R30° CO I-V curves used in LEED analysis. (Those few profiles with little structural information are now shown.)

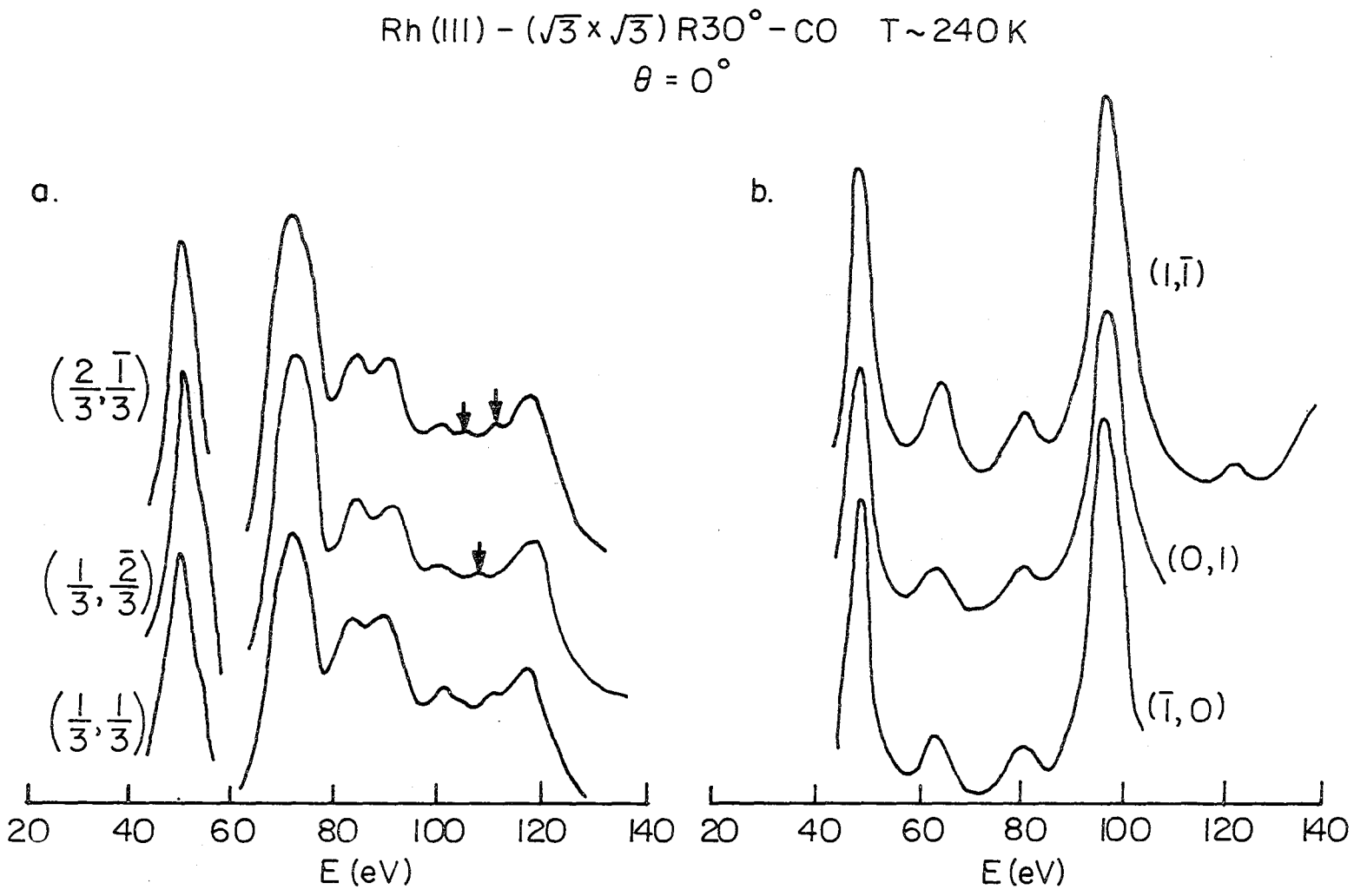
Rh (111) - (√3 x √3) R30° - CO T ~ 240 K
θ = 0°
a.
b.
(2/3, 1̄/3)
(1/3, 2̄/3)
(1/3, 1/3)
(1,1̄)
(0,1)
(1̄,0)
20 40 60 80 100 120 140
E (eV)
20 40 60 80 100 120 140
E (eV)
XBL 808-5664

Fig. 1

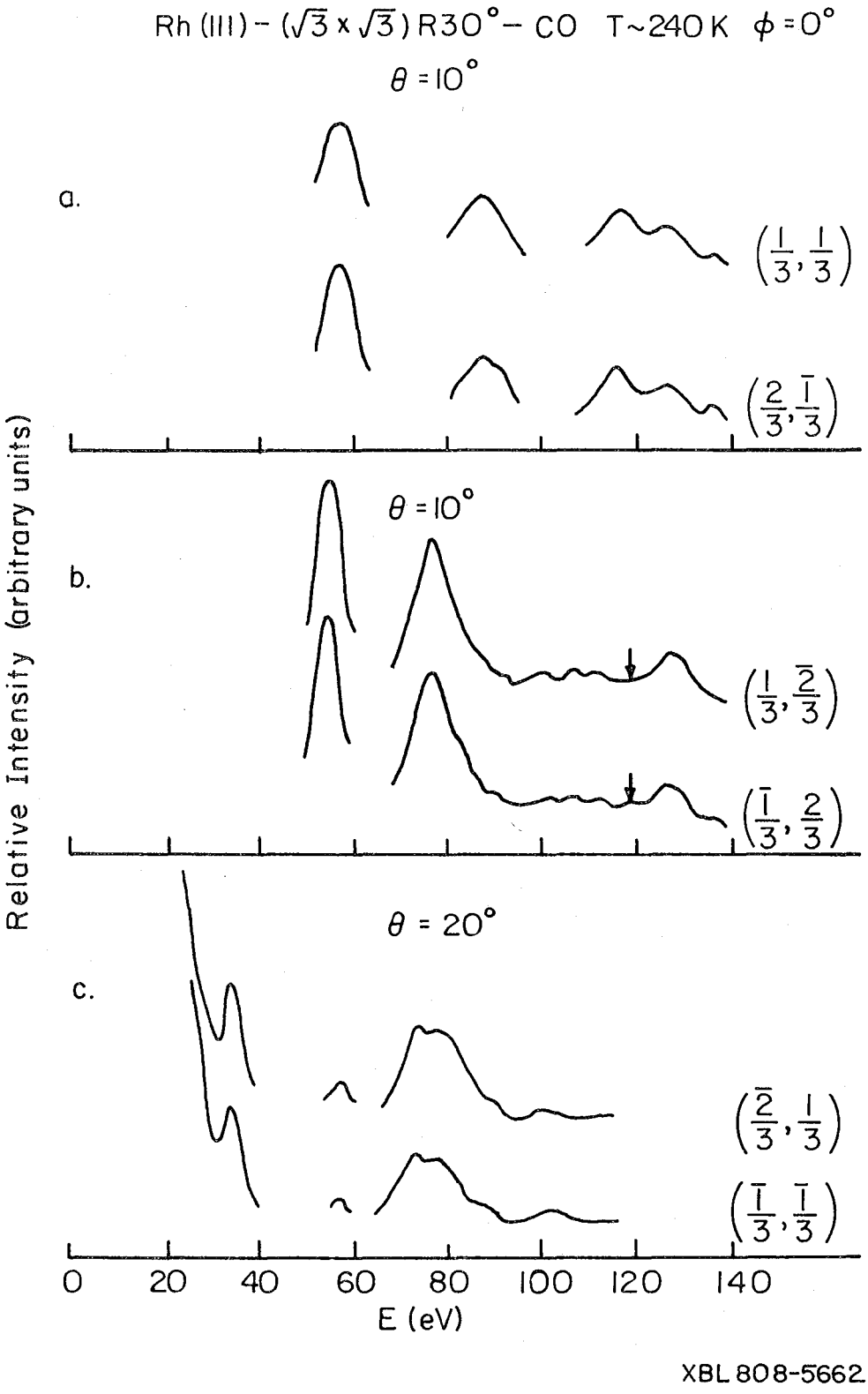

XBL 808-5662

Fig.2

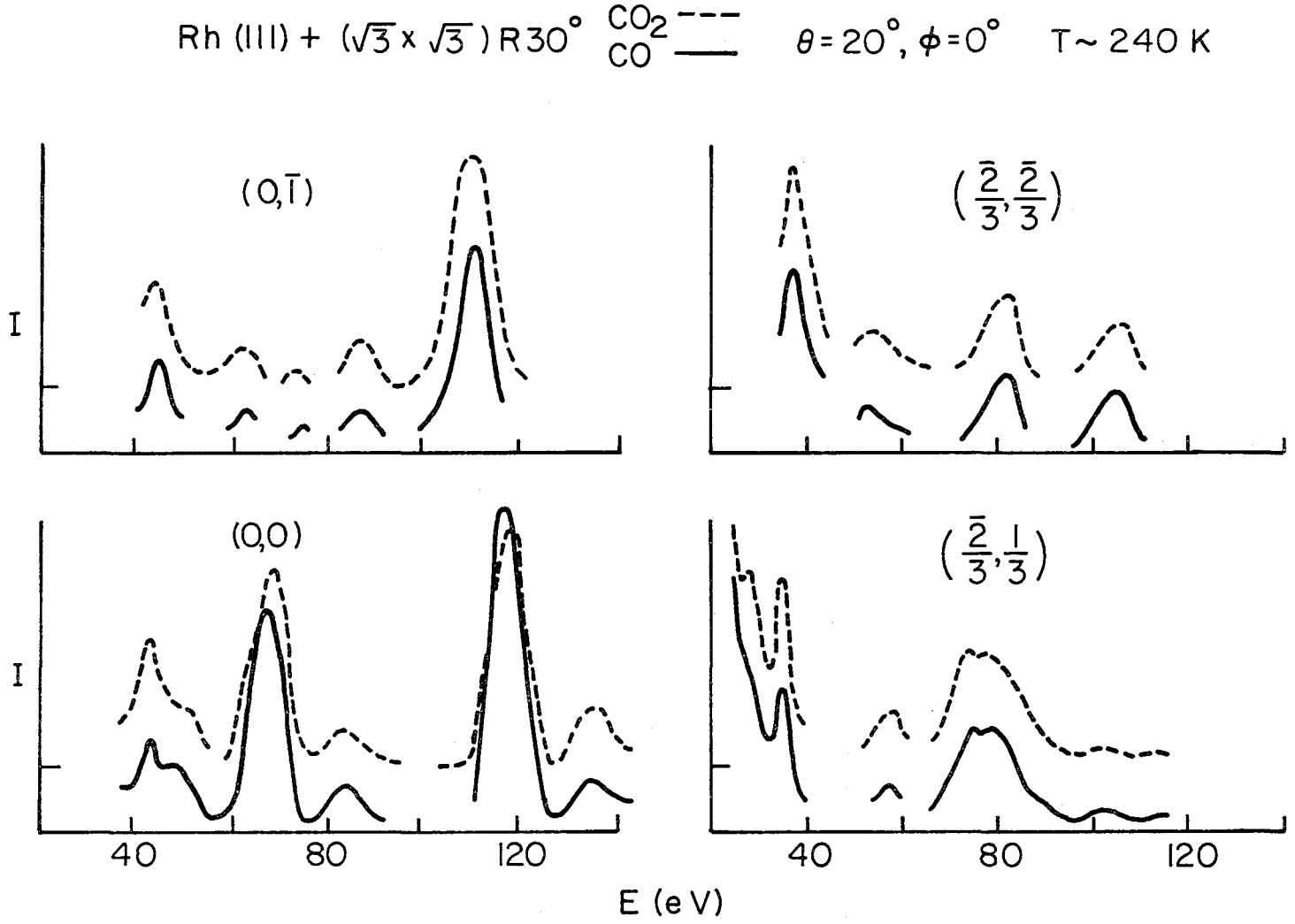

XBL 808-5661

Fig. 3

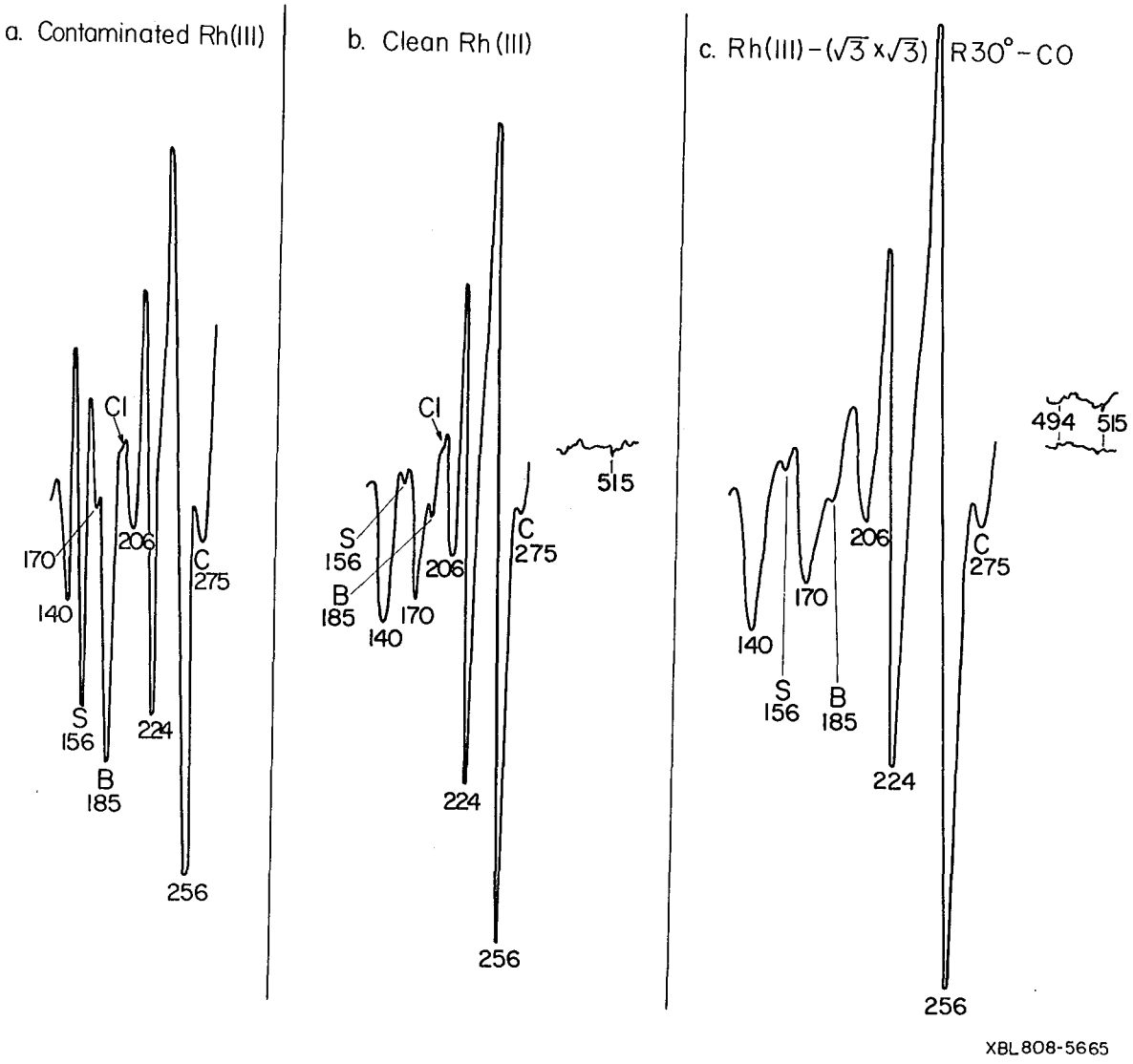
a. Contaminated Rh(III)
b. Clean Rh (III)
c. Rh(III) - (√3 x √3) R30° - CO
CI
170
140
206
C
275
S
156
224
B
185
256
515
494
XBL808-5665

Fig.4

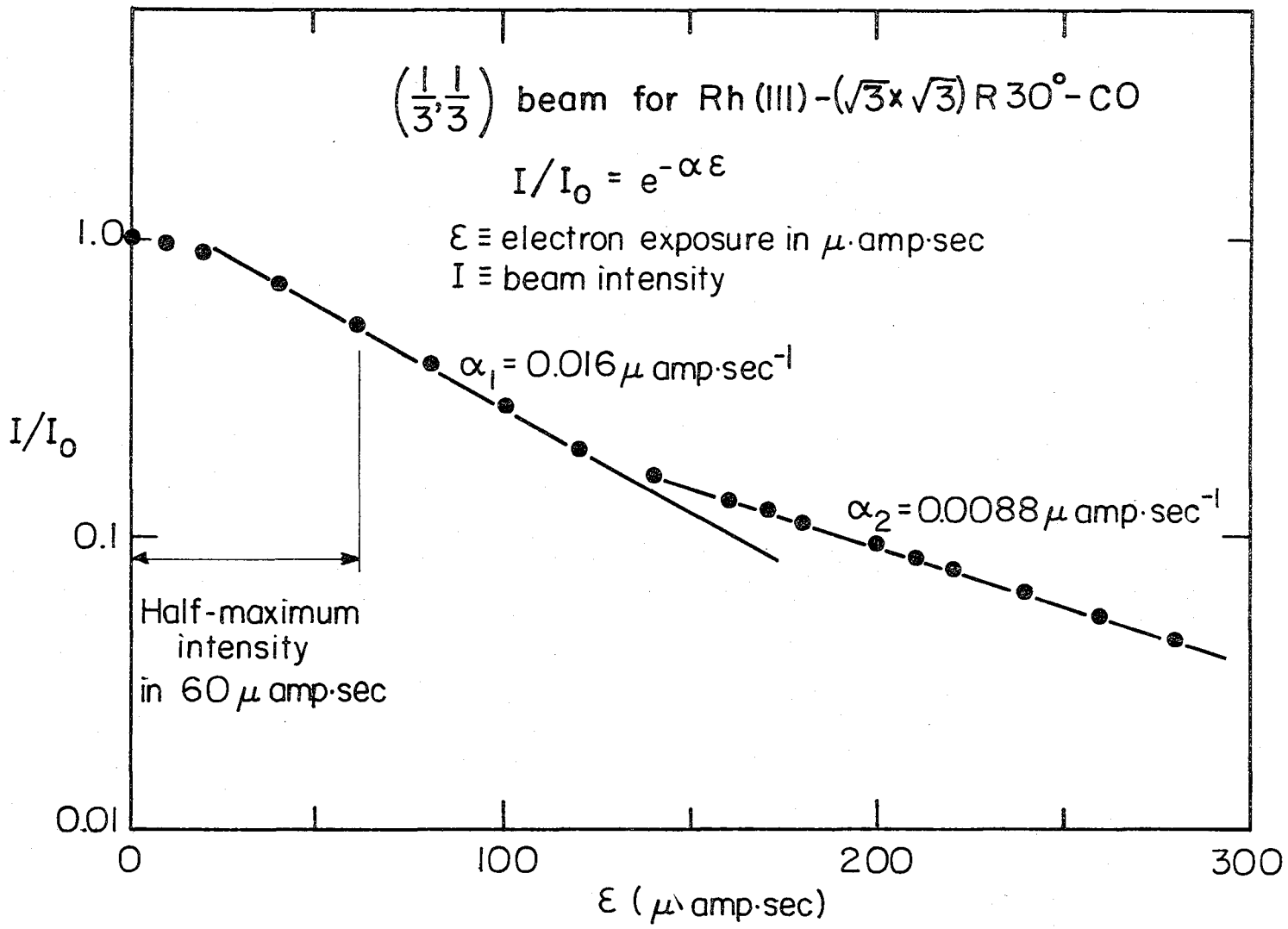

XBL808-5663

Fig.5

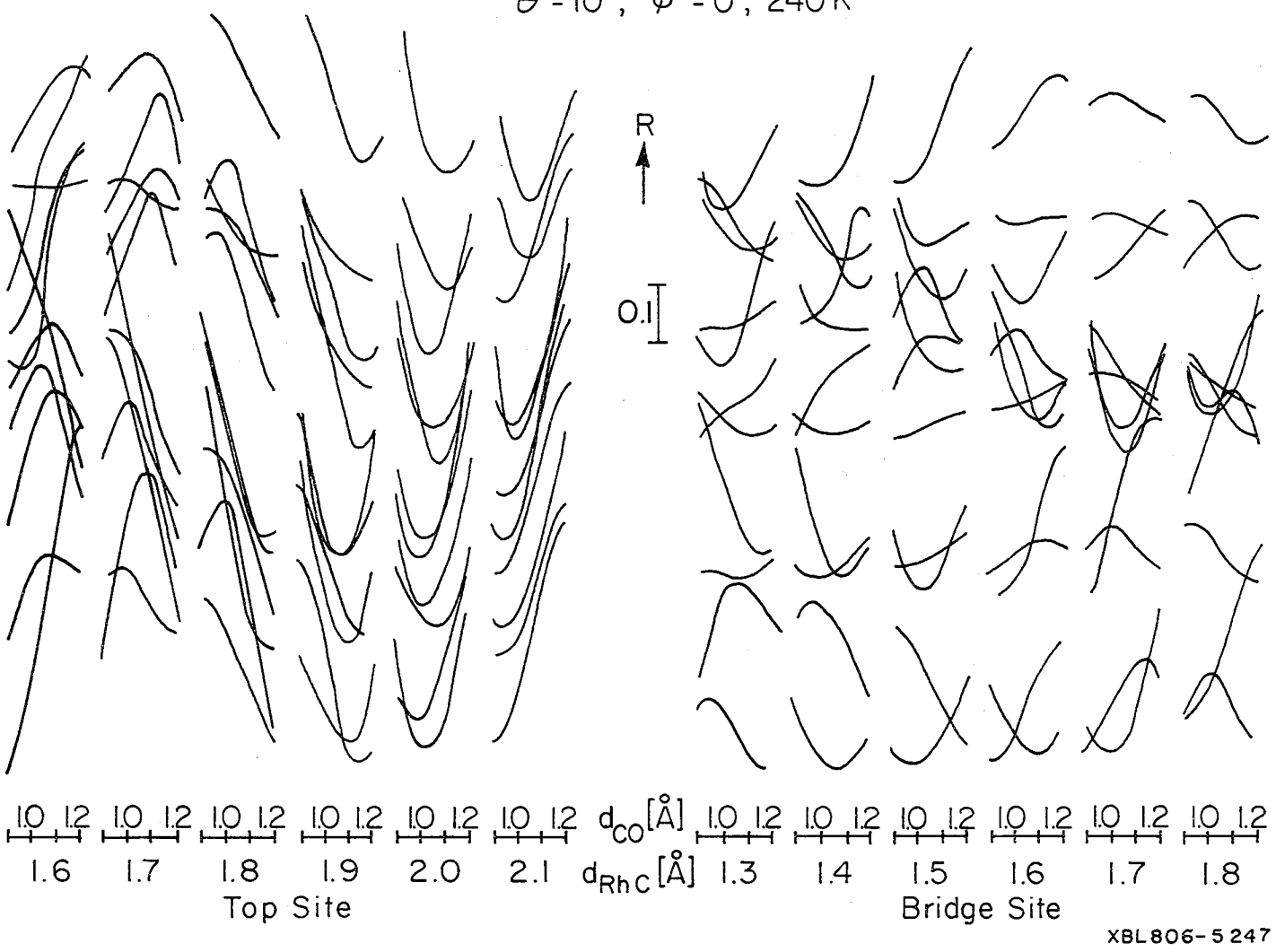
Rh (111) + (√3 x √3) R 30° CO
θ = 10°, φ = 0°, 240 K
R
0.1
1.0 1.2
1.6 1.7 1.8 1.9 2.0 2.1
d_CO [Å]
d_RhC [Å]
1.3 1.4 1.5 1.6 1.7 1.8
Top Site
Bridge Site
XBL806-5247

Fig. 6

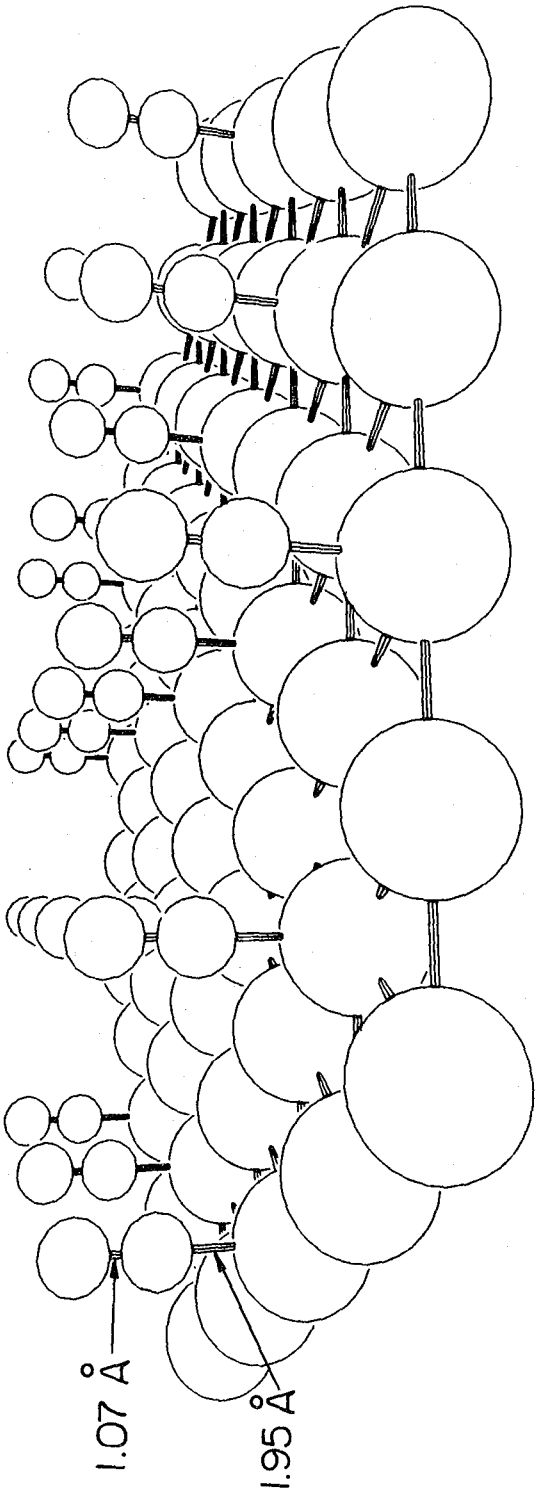

Fig.7

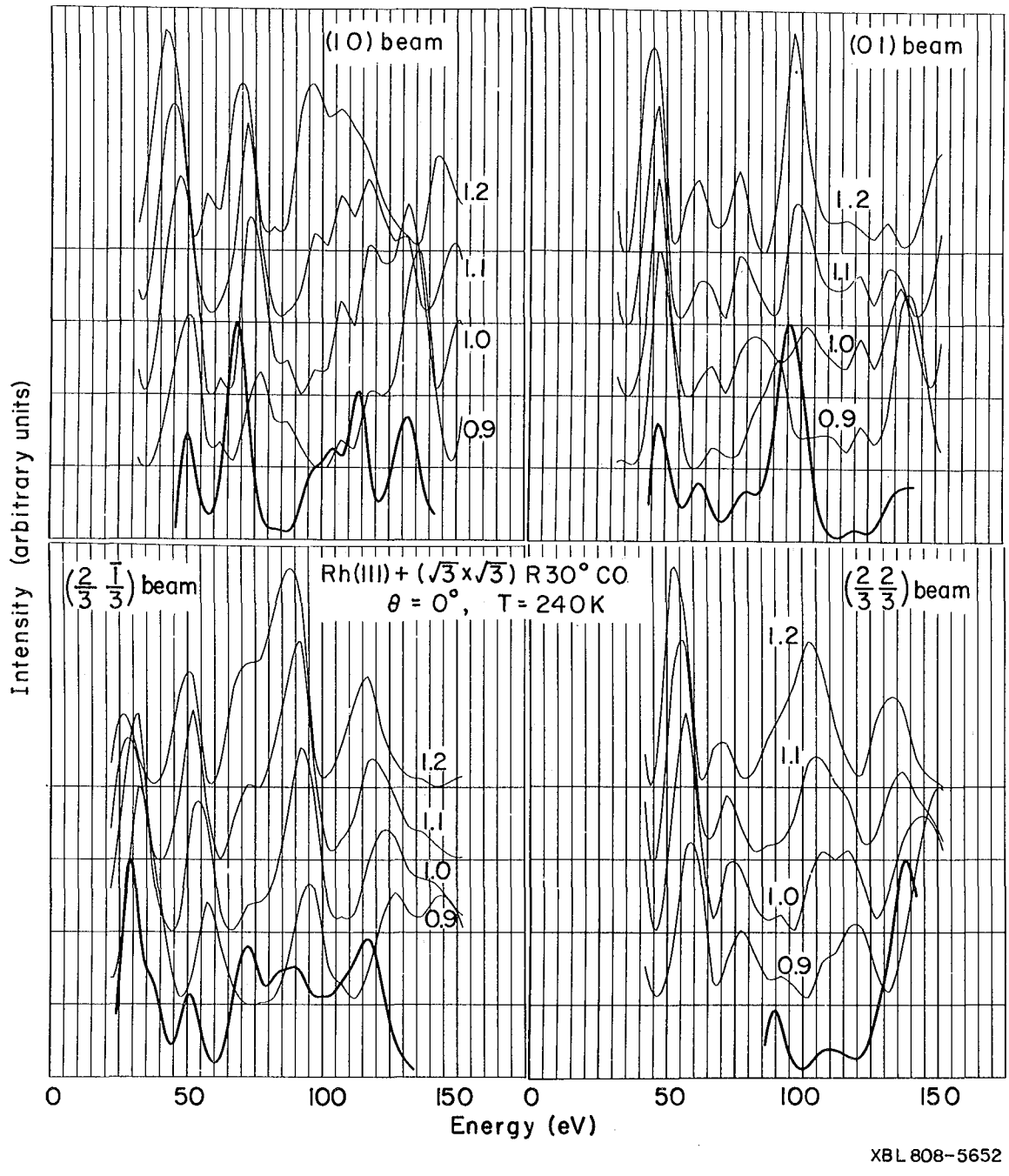
(1 0) beam
(0 1) beam
1.2
1.1
1.0
0.9
Rh(111) + (√3 x √3) R30° CO
θ = 0°, T = 240 K
(2/3 1̄/3) beam
(2/3 2/3) beam
Intensity (arbitrary units)
0
50
100
150
Energy (eV)
XBL 808-5652

Fig.8a

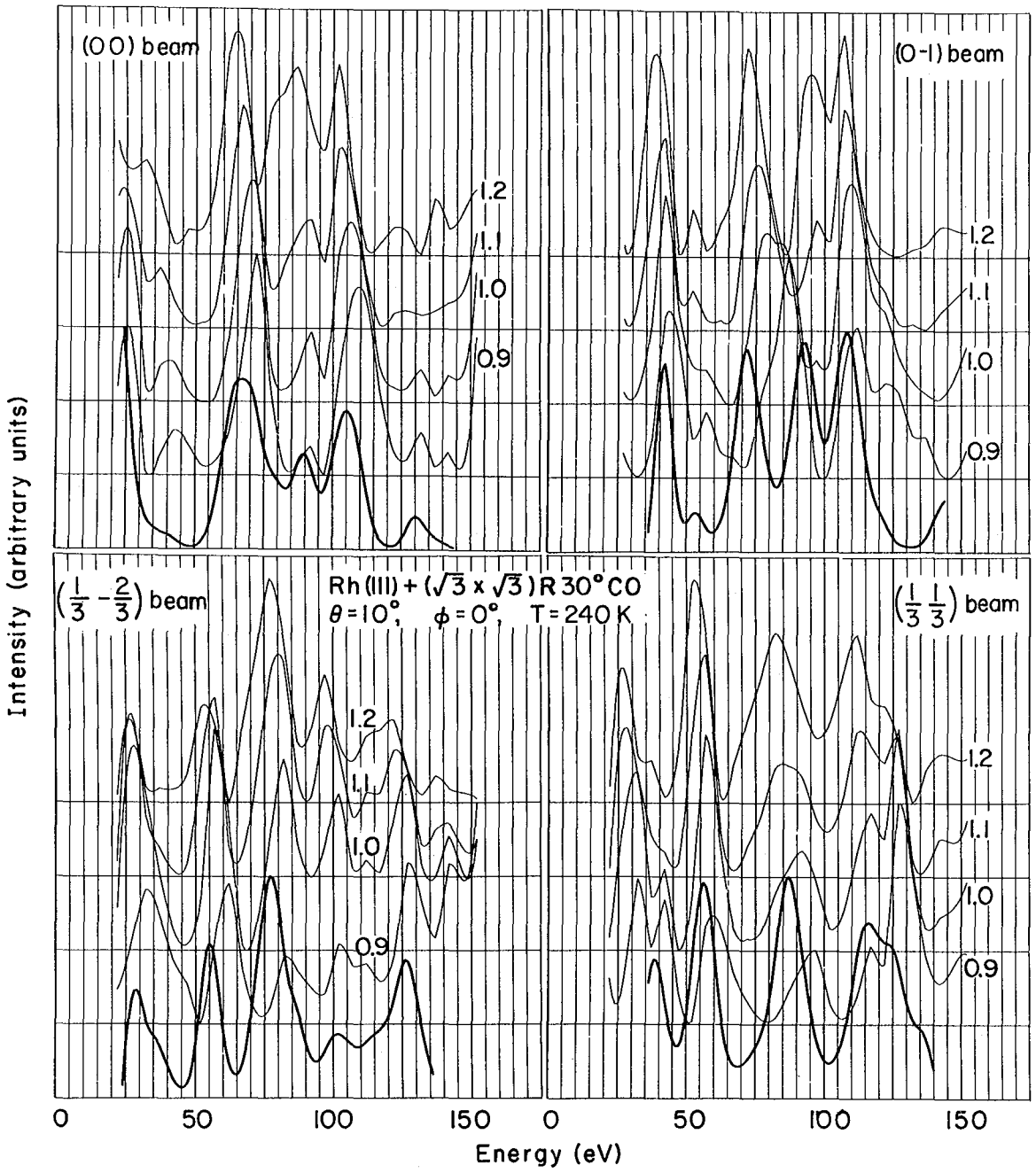
(00) beam
(0-1) beam
(1/3 -2/3) beam
(1/3 1/3) beam
Rh(111) + (√3 x √3)R30° CO
θ = 10°, φ = 0°, T = 240 K
1.2
1.1
1.0
0.9
Intensity (arbitrary units)
0
50
100
150
Energy (eV)
XBL 808-5651

Fig.8b

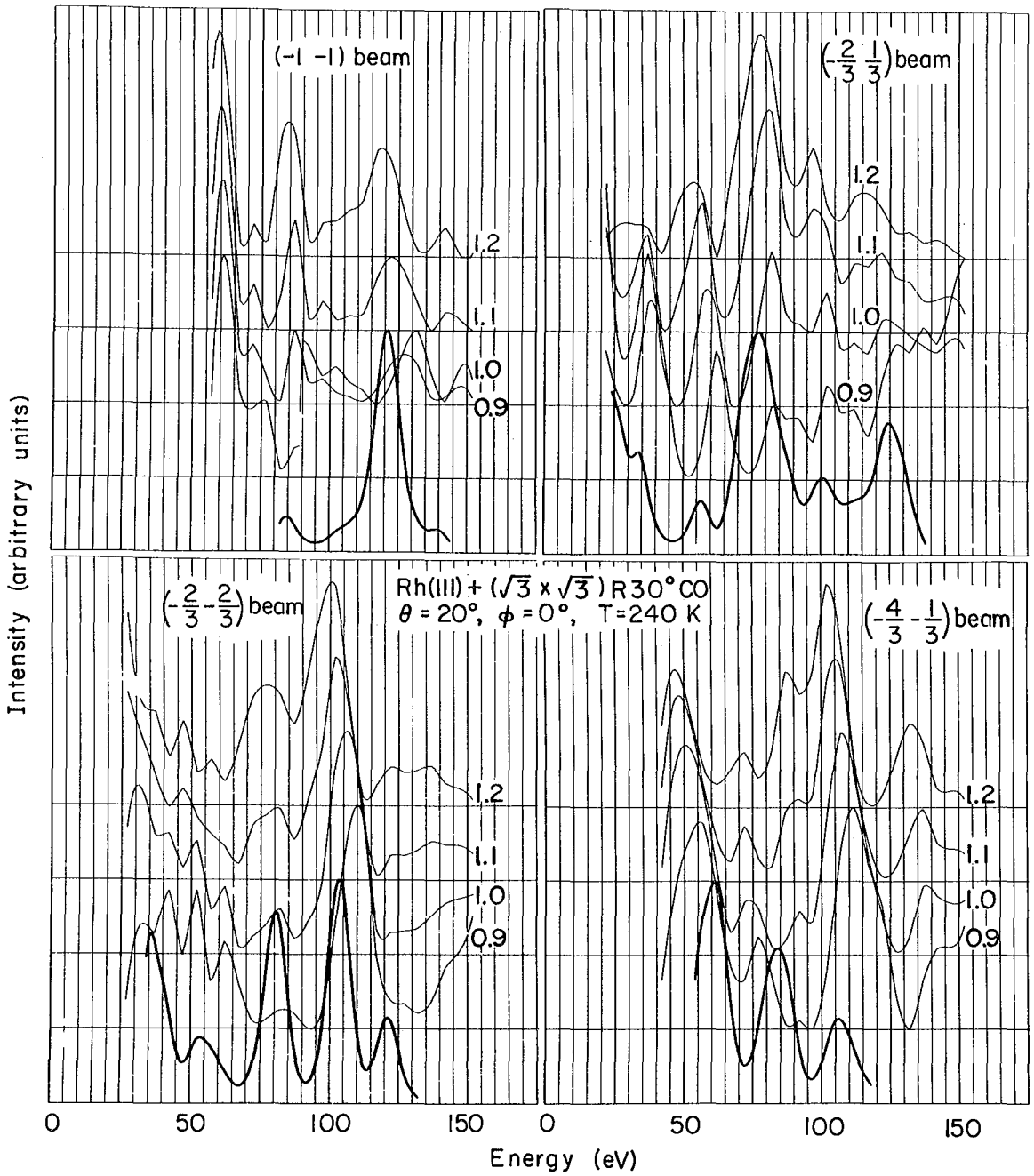

XBL808-5650

Fig.8c

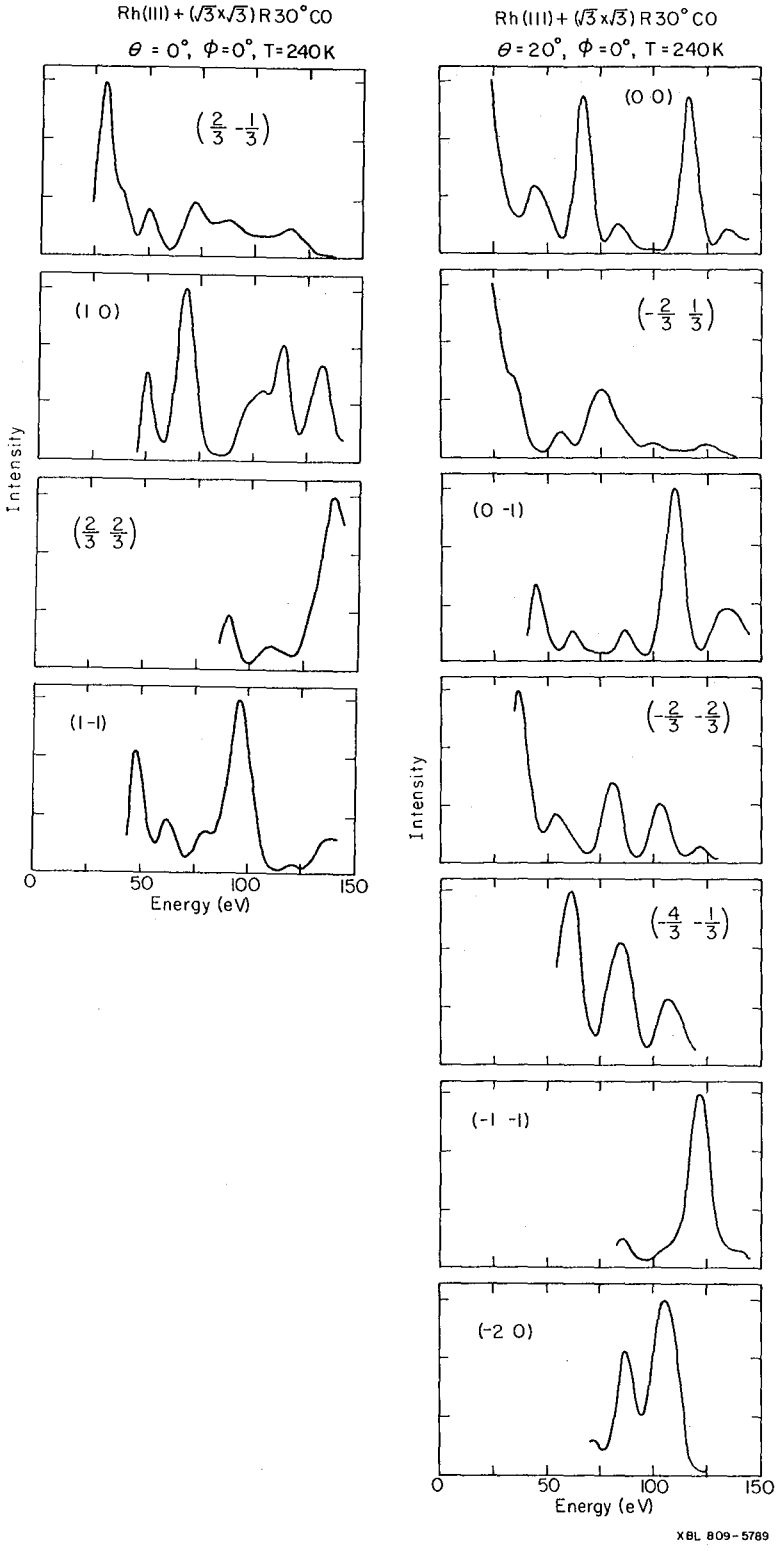
Rh(111) + (√3x√3) R30° CO
θ = 0°, Φ=0°, T=240K
(2/3 -1/3)
(1 0)
(2/3 2/3)
(1 -1)
Intensity
0
50
100
150
Energy (eV)
Rh(111) + (√3x√3) R30° CO
θ=20°, Φ=0°, T=240K
(0 0)
(-2/3 1/3)
(0 -1)
(-2/3 -2/3)
(-4/3 -1/3)
(-1 -1)
(-2 0)
Intensity
0
50
100
150
Energy (eV)
XBL 809-5789

App.1

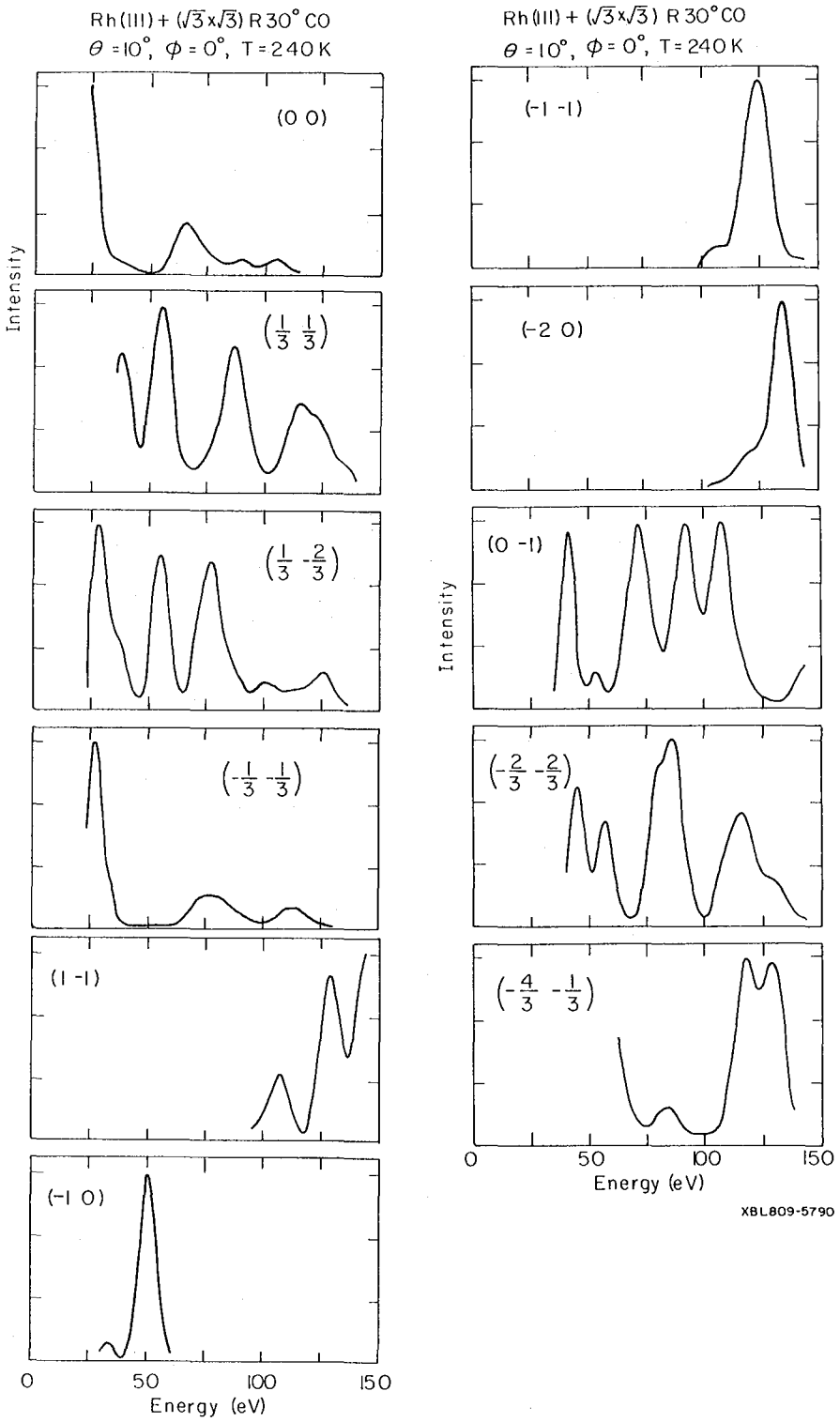
Rh(111) + (√3x√3) R30° CO
θ = 10°, φ = 0°, T = 240 K
(0 0)
(1/3 1/3)
(1/3 -2/3)
(-1/3 -1/3)
(1 -1)
(-1 0)
Intensity
0
50
100
150
Energy (eV)
Rh(111) + (√3x√3) R30° CO
θ = 10°, φ = 0°, T = 240 K
(-1 -1)
(-2 0)
(0 -1)
(-2/3 -2/3)
(-4/3 -1/3)
Intensity
0
50
100
150
Energy (eV)
XBL809-5790

TABLE I

Summary of LEED and HRELS Results for CO Adsorption

Substrate	Rh(111) [8]	Pd(100) [2]	Ni(100) [1,21]	Cu(100) [1,22]
Adsorption site	bridge	atop	atop	atop
Interlayer spacings	d_{PdC} = 1.93 Å	d_{NiC} = 1.71 Å	d_{CuC} = 1.90 Å	D_{RhC} = 1.95 Å
LEED pattern	$(2\sqrt{3}x\sqrt{2})R45°$	c(2x2)	c(2x2)	$(\sqrt{3}x\sqrt{3})R30°$
Co, RhC stretching frequency	236, 42 me V	256.5, 50.5		248, 57
Temperature	330-340 K	295 K	295 K	300 K

Note: proposed rule[20]

1. ν_{CO} < 230 meV, 3-fold hollow site
2. 230 < ν_{CO} < 248 MeV, 2-fold bridge site
3. ν_{CO} > 248 meV, atop site.

This report was done with support from the Department of Energy. Any conclusions or opinions expressed in this report represent solely those of the author(s) and not necessarily those of The Regents of the University of California, the Lawrence Berkeley Laboratory or the Department of Energy.

Reference to a company or product name does not imply approval or recommendation of the product by the University of California or the U.S. Department of Energy to the exclusion of others that may be suitable.